IOP Publishing Science and Technology of Advanced Materials
Sci. Technol. Adv. Mater. **9** (2008) 045009 (10pp) doi:10.1088/1468-6996/9/4/045009

Effect of zinc phosphate chemical conversion coating on corrosion behaviour of mild steel in alkaline medium: protection of rebars in reinforced concrete

Florica Simescu and Hassane Idrissi

Laboratoire MATEIS UMR CNRS 5510, Equipe RI_2S INSA - Lyon, Bât. L. Vinci, 21 Av. Jean Capelle, 69621, Villeurbanne Cedex, France

E-mail: Hassane.Idrissi@insa-lyon.fr

Received 8 July 2008
Accepted for publication 25 September 2008
Published 19 December 2008
Online at stacks.iop.org/STAM/9/045009

Abstract
We outline the ability of zinc phosphate coatings, obtained by chemical conversion, to protect mild steel rebars against localized corrosion, generated by chloride ions in alkaline media. The corrosion resistance of coated steel, in comparison with uncoated rebars and coated and uncoated steel rebars embedded in mortar, were evaluated by open-circuit potential, potentiodynamic polarization, cronoamperometry and electrochemical impedance spectroscopy. The coated surfaces were characterized by x-ray diffraction and scanning electron microscopy. First, coated mild steel rebars were studied in an alkaline solution with and without chloride simulating a concrete pore solution. The results showed that the slow dissolution of the coating generates hydroxyapatite $Ca_{10}(PO_4)_6(OH)_2$. After a long immersion, the coating became dense and provided an effective corrosion resistance compared with the mild steel rebar. Secondly, the coated and uncoated steel rebars embedded in mortar and immersed in chloride solution showed no corrosion or deterioration of the coated steel. Corrosion rate is considerably lowered by this phosphate coating.

Keywords: steel corrosion, rebar protection, alkaline medium, phosphate coating, hydroxyapatite

(Some figures in this article are in colour only in the electronic version)

1. Introduction

Steel rebars in concrete are protected against corrosion by an oxide protective layer, called the passive layer, formed by the alkalinity of a concrete pore solution (pH close to 13). The localized attack of this protective layer leads to an expansion in the cross section of the reinforcement due to the formation of high-volume corrosion products. This process can lead to the cracking or spalling of concrete and a dangerous loss of structural stability. The most common cause of the corrosion of marine structures, marine garages, and bridge decks is attack of chlorides present in salts. The effect of Cl^- ions in depassivating steel surfaces even at high pH can be seen as a function of the net balance between two competing process: the stabilization (and repair) of the film by OH^- ions and the damage of the film by Cl^- ions [1].

Thus, many studies have been performed to determine the best method of preventing corrosion in reinforcing bars [2, 3]. Among the possible anticorrosion methods, the use of phosphated reinforcing bars is commonly employed to extend the lifetime of such rebars in concrete structures [2, 4]. The literature shows that the alkaline

Table 1. Composition and pH of the phosphating bath.

Composition	pH
Zn^{2+} (0.07 M) + PO_4^{3-} (0.15 M) + Ni^{2+} (0.017 M) + NO_3^- (0.05 M)	2.1
	2.1

Table 2. Description of various electrolytes used.

Solution	$Ca(OH)_2$ (mol L^{-1})	NaOH (mol L^{-1})	KOH (mol L^{-1})	NaCl (g L^{-1})	pH
S	Saturation	0.001	0.001	0	12.6
SC	Saturation	0.001	0.001	35	12.5

stability of phosphate coatings depends on their chemical composition and crystal structure [5]. These phosphate coatings are generally composed of hopeite $Zn_3(PO_4)_2 \cdot 4H_2O$ and phosphophyllite $Zn_2Fe(PO_4)_2 \cdot 4H_2O$. Hopeite has a higher alkaline solubility than phosphophyllite [6–10]. Thus, alkaline solutions first dissolve the coating composed of hopeite. Then, the dissolution continues for layers rich in iron and those mainly composed of phosphophyllite [11].

There are few published fundamental studies of the alkaline stability of the phosphate coating, particularly in Ca^{2+}-saturated solution.

The aim of this work is to develop zinc phosphate coatings on reinforcing bars to study their stability and corrosion behaviour in alkaline solutions. Synthetic media, saturated with Ca^{2+} ions, was used to simulate the aqueous solution existing in concrete pores at early stages, and chloride ions were added to simulate degraded concrete. These tests, in simulated concrete pore solutions are necessary to understand the protection ability of zinc phosphate coatings, prior to their application on reinforcing bars embedded in concrete.

2. Experimental

2.1. Substrate and coating

Experiments were conducted using mild steel bars (with 0.2 wt.% C, and with a diameter of 8 mm), denoted MS. The phosphated surface (denoted PMS) was approximated as a cylinder with a height of 2 cm corresponding to a surface area of 5.5 cm^2. The surfaces were chemically pickled with 36.5% HCl for 1 min, and then rinsed 3 times with deionized water. After rinsing, the samples were immersed in a phosphating bath. Chemical conversion treatment (denoted CC) was performed in the phosphating bath (pH = 2.1) for 10 min at 55 °C. The bath composition is given in table 1. After the phosphate treatment, the samples were rinsed with deionized water and dried in ambient air.

2.2. Electrolytes

The PMS and MS samples were immersed in alkaline solutions simulating the concrete interstitial electrolyte at ambient temperature (table 2). A saturated calcium hydroxide (denoted S) solution was used to simulate the aqueous alkaline content of the concrete pore solutions, with an approximate pH of 12.6. To simulate the aqueous phase of concrete contaminated by chloride, 35 g L^{-1} NaCl was added to the S solution to obtain an electrolyte denoted SC. The pH of the solution containing chloride was 12.5.

Table 3. Composition of mortar.

Component	Weight (g)
Water/cement	0.5
Water	225
Portland cement	450
Normal sand	1350

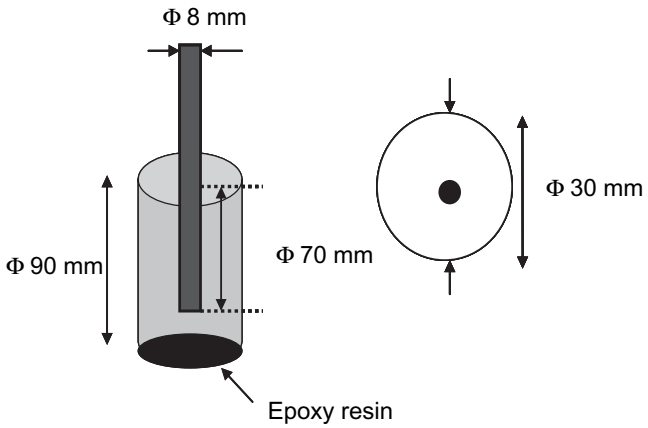

Figure 1. Reinforced mortar specimen.

2.3. Reinforced mortar specimens

The coated and uncoated steel rebars were embedded in standard mortar (water/cement = 0.5). The composition of this mortar is given in table 3.

The samples were defined of their dimensions in a way representative of actual structures. They were cylinders of 30 mm diameter and 90 mm height (figure 1).

After mixing water, cement and sand, the paste produced was poured into a PVC moulding in which a coated or uncoated mild steel, was placed according to its longitudinal axis. The samples were compacted using a vibrating table for 60 s, then dried in air for 28 days. After the samples were removed from the PVC moulding, an epoxy resin coating was applied to the lower face of the sample to ensure the infiltration of the solution only through the lateral surface.

2.4. Electrochemical measurements

Different electrochemical techniques were used to evaluate the corrosion behaviour of the PMS and MS samples: open-circuit potential (denoted E_{corr}), and potentiodynamic polarization measurements, and electrochemical impedance spectroscopy (EIS). E_{corr} was monitored for 8 days. Polarization curves ($I = f(E)$) were plotted at a scan rate of 0.1 mV s^{-1} from −100 mV to 1000 mV versus E_{corr} in the anodic direction. EIS was carried out at a corrosion potential with a frequency variation between 100 kHz and 0.01 Hz and

Table 4. PMS composition.

Element wt.%	O	P	Fe	Zn
PMS composition	7.0 ± 1.0	8.7 ± 1.0	24.7 ± 1.0	59.6 ± 1.0

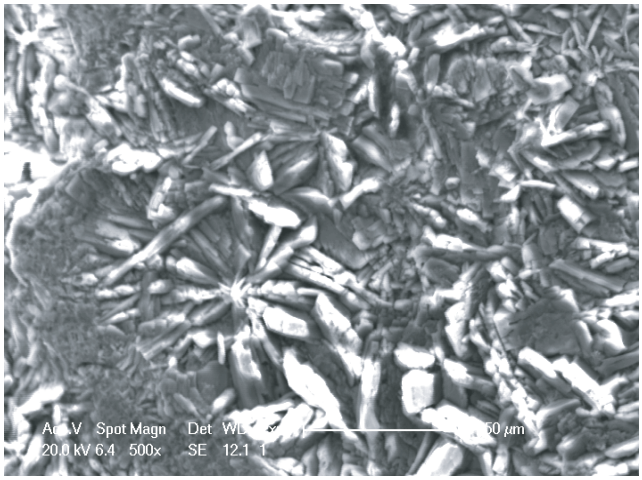

Figure 2. SEM images of mild steel coated surface.

a potential sine signal of 10 mV. Impedance data were fitted using ZImp software.

The reinforced mortar specimens were immersed in sodium chloride solution (3.5%). Corrosion was accelerated by an imposed potential of 400 mV SCE^{-1} [1] and current density was monitored by cronoamperometry for 8 days.

2.5. Surface analysis

The morphology and coating compositions were studied by scanning electron microscopy (SEM) in the secondary electron imaging (SEI) and energy dispersive spectroscopy (EDS) modes. The coating crystallographic structure was analysed by x-ray diffraction (XRD) analysis using $Cu_{K-L(2,3)}$ radiation.

3. Results and discussion

3.1. Morphology and composition of the coating

The SEM shows that the coating is compact, well-crystallized and completely covers the steel surface (figure 2). The structure is characterized by small needles with sizes up to 8 μm. The EDS shows that the coating composition is 60 wt.% zinc and 9 wt.% phosphorus (table 4).

The x-ray diffraction analysis performed on the coated steel indicates the presence of two phases: hopeite $Zn_3(PO_4)_2 \cdot 4H_2O$ and phosphophyllite $Zn_2Fe(PO_4)_2 \cdot 4H_2O$ (figure 3). The presence of the phosphophyllite phase is related to the MS dissolution in the acid bath (pH = 2.2) during the phosphate treatment [12–14]. According to Donofrio [6], the possible reactions (equations (1) and (2)) for the hopeite and phosphophyllite formations are

$$3Zn^{+2} + 2H_2PO_4^- + 4H_2O \rightarrow Zn_3(PO_4)_2 \cdot 4H_2O + 4H^+, \quad (1)$$

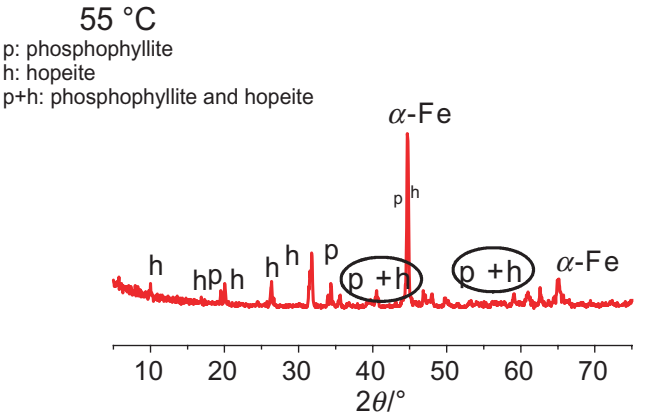

Figure 3. X-ray diffraction pattern of PMS.

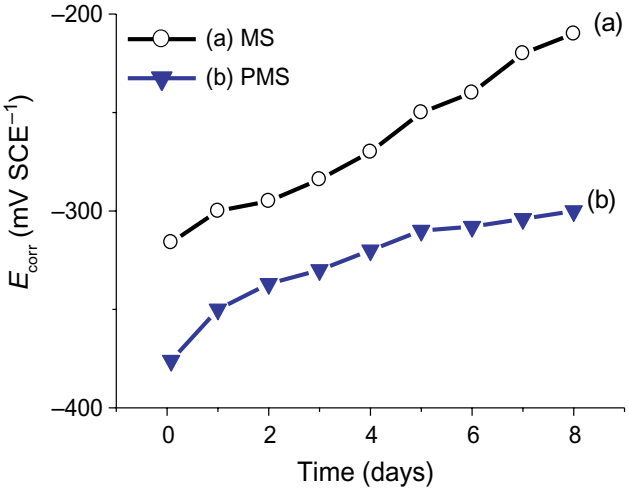

Figure 4. E_{corr} evolution for (a) MS and (b) PMS in S solution.

$$2Zn^{+2} + Fe^{+2} + 2H_2PO_4^- + 4H_2O \rightarrow Zn_2Fe(PO_4)_2 \cdot 4H_2O + 4H^+. \quad (2)$$

3.2. Corrosion behaviour in alkaline medium (pH 12.6)

3.2.1. Corrosion potential evolution. The E_{corr} monitoring of the PMS and MS samples shows a trend toward values higher than those recorded during the immersion. For the MS sample (figure 4(a)), the corrosion potential after passivation is approximately −250 to −300 mV SCE^{-1} [15]. Thus, after three days of immersion in the S solution, E_{corr} is stabilized in the passive region throughout the test period. For the coated steel, E_{corr} increases to −300 mV SCE^{-1} This indicates a slow dissolution of the coating without resulting in uncovered steel zones. Indeed, the coating is dissolved rapidly in NaOH/KOH solutions [5]; in our medium, the presence of calcium is responsible for the slow dissolution of the coating and for the obtained trend of the corrosion potential curves.

3.2.2. Polarization curves. Figure 5 shows the polarization curves of the PMS and MS specimens after 8 days of immersion in the S solution. It is shown that an extended

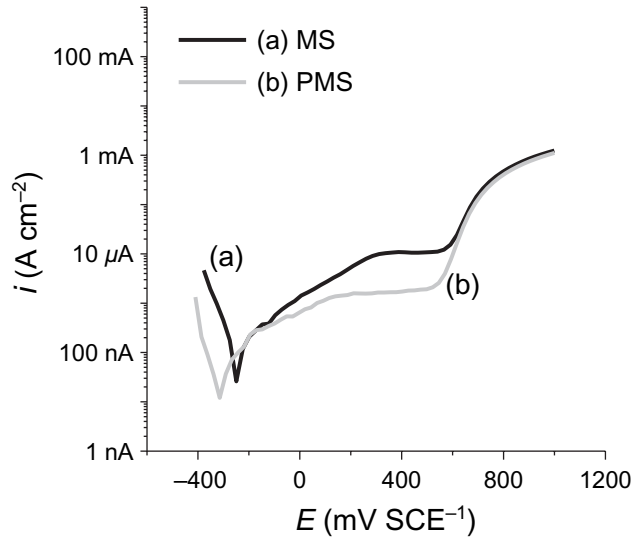

Figure 5. Polarization curves for MS and PMS after 8 days of immersion in S solution.

passive region exists in the anodic polarization part for the uncontaminated chloride solution. This region starts immediately after E_{corr} and continues up to the pitting potential (E_{pit}) at ~560 mV SCE^{-1} (for both specimens). PMS has a lower passive current density (about 0.8 μA cm^{-2}) than MS (about 8 μA cm^{-2}) (table 5). PMS has a lower current density that MS, which can be related to the difference in nature between their passive layers, because a zinc phosphate coating is applied on the surface. It can be concluded that PMS in a Ca^{2+}-saturated solution has a higher stability than MS, and that the zinc phosphate coating has an extra corrosion resistance to MS after 8 days of immersion.

Table 5. Corrosion potentials, current densities (at corrosion potential) and pitting potentials of MS and PMS specimens after 8 days of immersion in S solution.

Sample	E_{corr} (mV ECS^{-1})	i (μA cm^{-2})	E_{pit} (mV ECS^{-1})
MS	−240	8	560
PMS	−320	0.8	556

3.2.3. Electrochemical impedance spectroscopy. The electrochemical impedance diagrams, at the corrosion potential, are obtained by EIS after 2 h, and 1, 4, 6 and 8 days of steel and coated steel immersions.

For the untreated steel, Nyquist plots and Bode diagrams are respectively presented in figures 6(a) and (b). The

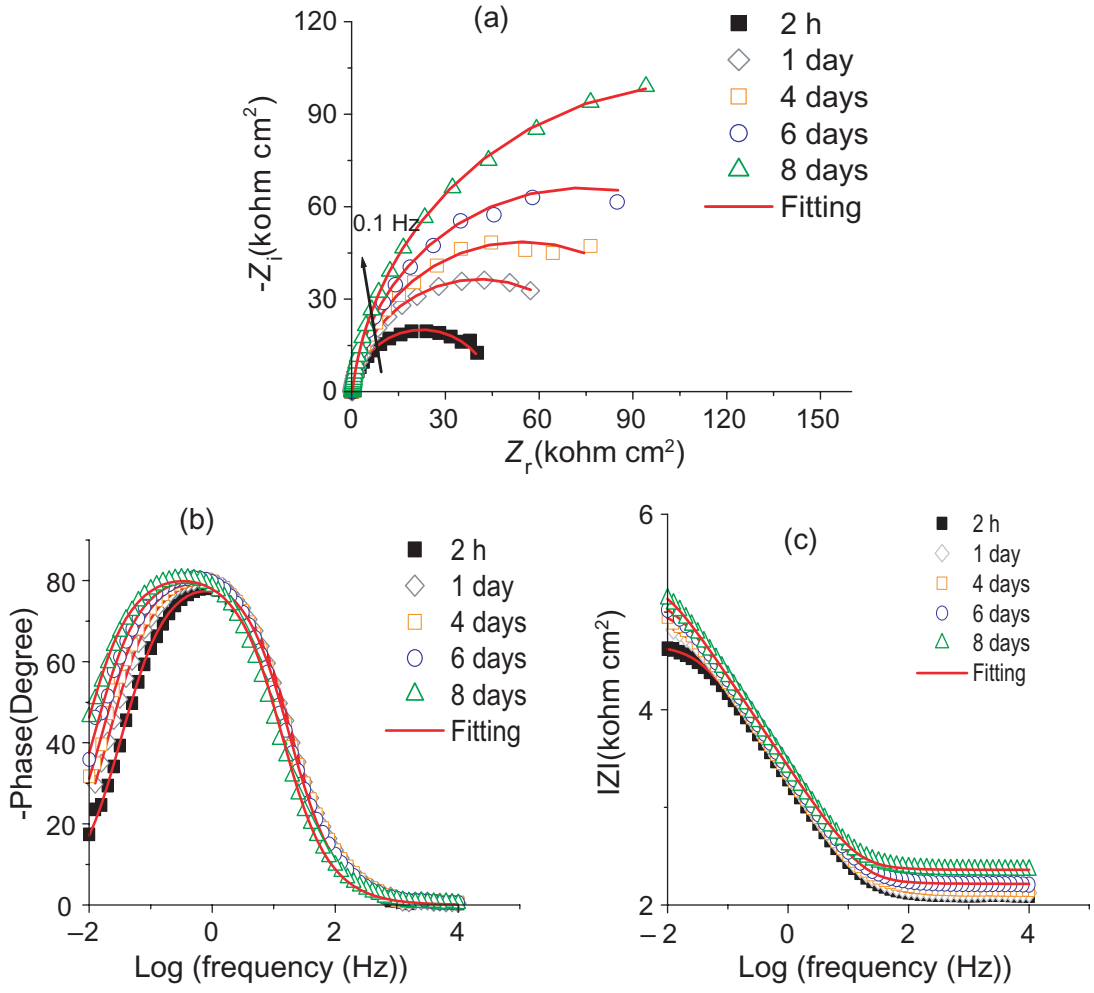

Figure 6. (a) Nyquist diagram and (b)–(c) Bode diagrams of MS from 2 h to 8 days of immersion in S solution: experimental values (dots) and fitted values (solid lines).

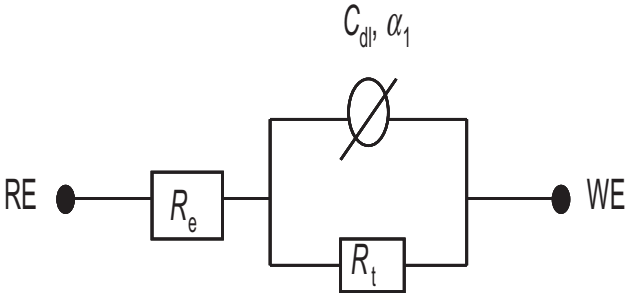

Figure 7. Equivalent circuit used for modelling the EIS data.

Table 6. Electrical parameters for MS immersed in S solution obtained through fitting EIS data.

Time (day)	R_t (kΩ cm^2)	α	C_{dl} (μF cm^{-2})	χ^2 (error factor)
0.08	44.5	0.93	66.9	5×10^{-3}
1	81.5	0.93	57.7	1×10^{-3}
4	109	0.93	55.2	1×10^{-3}
6	142	0.93	53.3	8×10^{-3}
8	223	0.93	50.6	2×10^{-3}

electrical parameters obtained through fitting EIS data using an electric equivalent circuit $R(QR)$ are listed in table 6. The proposed electric equivalent circuit is given in figure 7 where $R_e \sim 190\ \Omega\text{cm}^2$ corresponds to the electrolyte resistance, while C_{dl} and R_t, respectively, represent the double-layer capacitance and charge transfer resistance of the steel/solution interface.

The above representations show one capacitive loop whose diameter increases with the time of immersion. Thus, R_t increases simultaneously with a decrease in C_{dl}. These evolutions characterize the blocking increase in the extent of charge transfer at the steel surface and the decrease in the area of the contact surface related to passive film formation.

Nyquist plots and Bode diagrams of the coated steel (PMS) are represented in figure 8. These EIS diagrams show two capacitive loops, even though one capacitive loop is clearly visible. Indeed, if we use a single circuit consisting of R and C in parallel, the electrical parameters obtained through fitting EIS data gives a systematic variation, indicating that the $R(QR)$ model is not adequate for this case. The first three

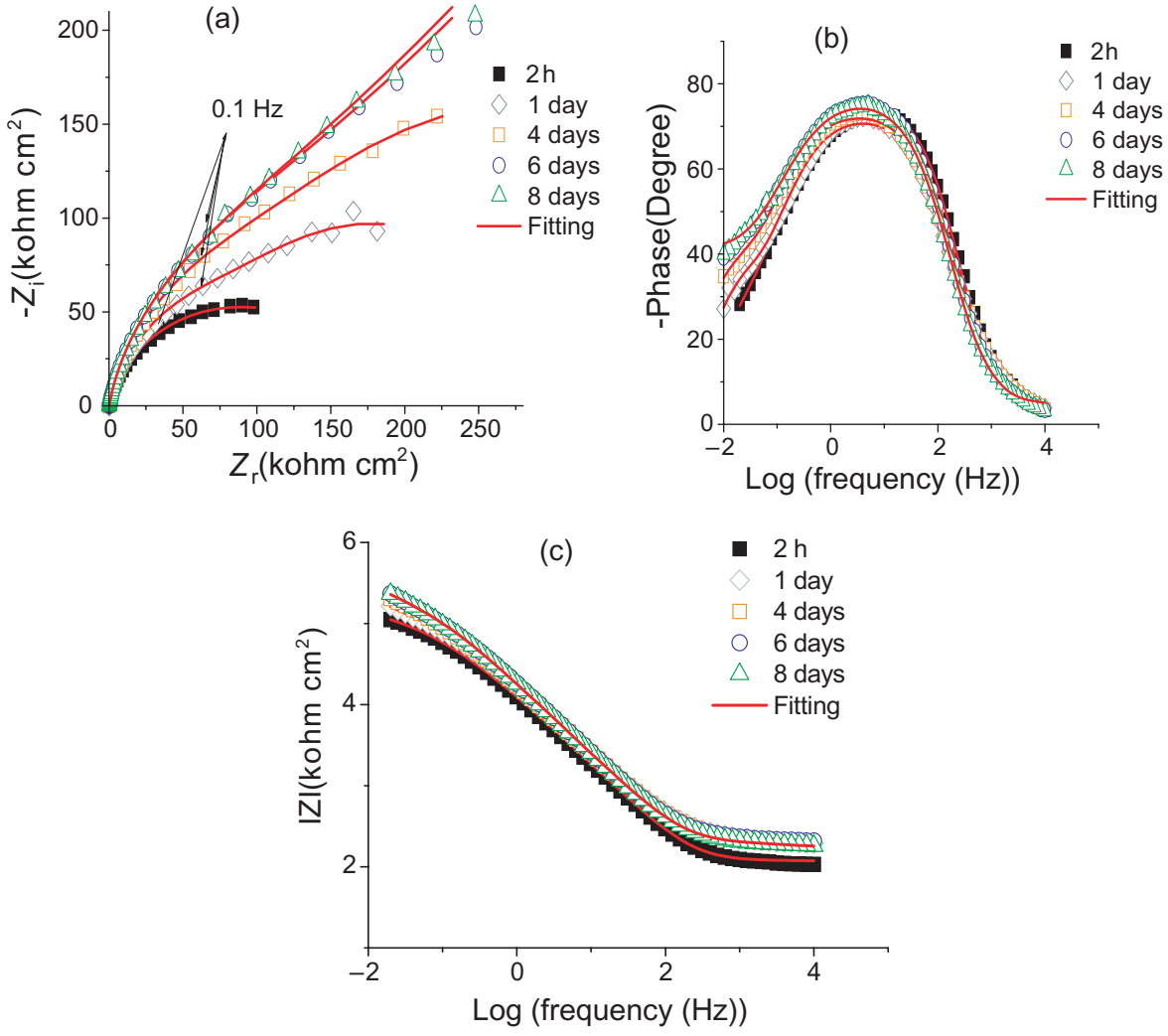

Figure 8. Nyquist (a) and (b)–(c) Bode diagrams of PMS from 2 h to 8 days of immersion in S solution: experimental values (dots) and fitted values (solid line).

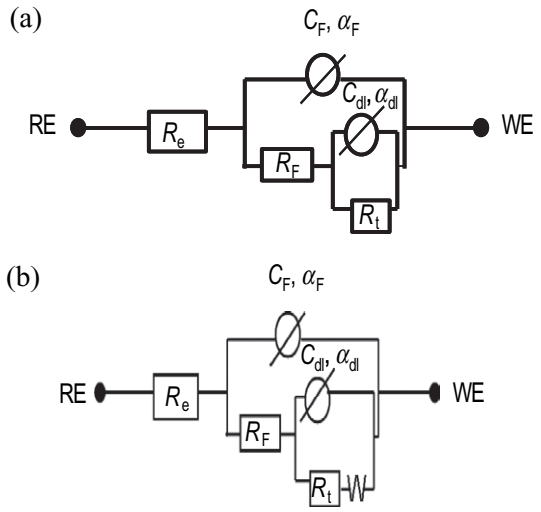

Figure 9. Equivalent circuit used for modelling the EIS data of PMS up to (a) 4 and (b) 6–8 days.

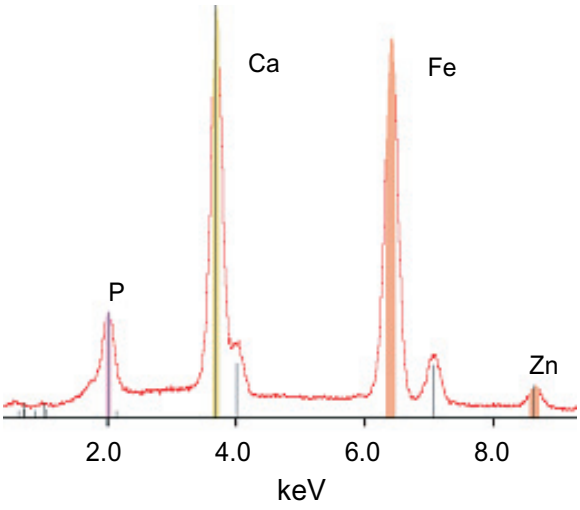

Figure 11. EDS composition of PMS after 8 days of immersion in S solution.

diagrams were modelled by an electric equivalent circuit with two time constants $R(Q(R(QR)))$ shown in figure 9(a), and the last two diagrams were modelled by the proposed electric circuit $R(Q(R(Q(RW))))$ shown in figure 9(b). In this case, the increase in film resistance (R_F) suggests the formation of a protective layer causing a decrease in the area of the active steel surface. In conjunction with this phenomenon, there is a capacity film reduction (C_F) that leads to a film thickness increase (equation (3)) expressed as

$$C_F = \varepsilon_0 \varepsilon_r A/d, \tag{3}$$

where ε_0 is the vacuum permittivity (8.85×10^{-14} F cm^{-1}), ε_r is the dielectric constant, A the active surface and d the thickness of film.

Indeed, these parameters indicate the existence of two time constants associated with two electric circuits: $R_F C_F$ and $R_t C_{dl}$. After four days of immersion, other elements relating to Warburg diffusion was observed [16, 17].

SEM images (figure 10) and results of the surface analyses (EDS and XRD) of the coated steel after 8 days of immersion in S solution reveal a different morphology for this protective coating. Crystal size decreases considerably during the 8-day immersion in a solution of pH 12.6. Indeed, even after one day of immersion, we observe the dissolution of zinc phosphate coating and the germination of small crystals.

During the eight days of immersion, the larger crystals remains unchanged morphologically, but were covered uniformly by small hexagonal plates (figure 10(b)). EDS analysis shows that, after 8 days of immersion, the coating became composed of P, Ca, Fe and very little Zn (figure 11).

The XRD analysis of these crystals (figure 12) shows the presence of low-intensity lines, related to the formation of small hexagonal crystals composed of hydroxyapatite $Ca_{10}(PO_4)_6(OH)_2$. This compound is stable in alkaline media (pH = 11–13), as was shown by Shih *et al* [18].

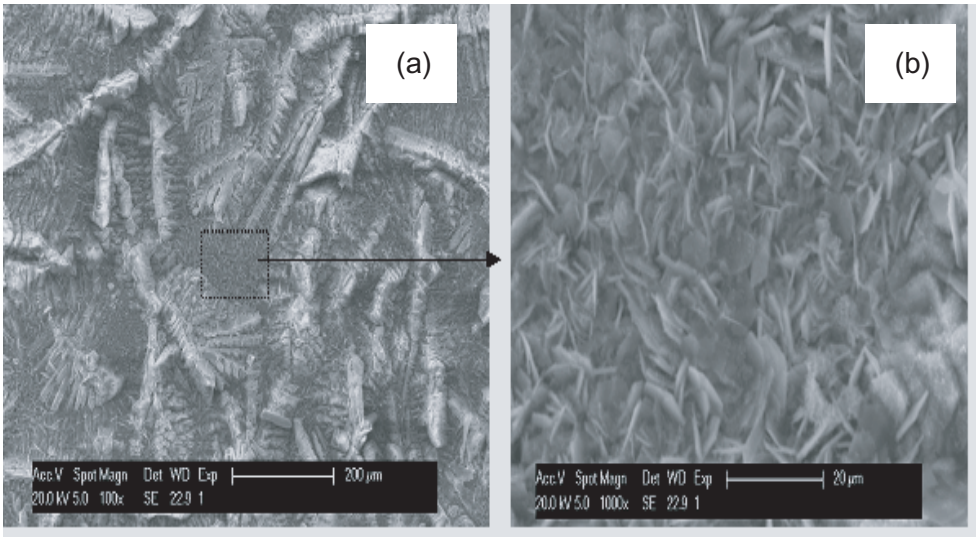

Figure 10. SEM images of PMS after 8 immersion days in S solution: (a) 200 and (b) 20 μm scales.

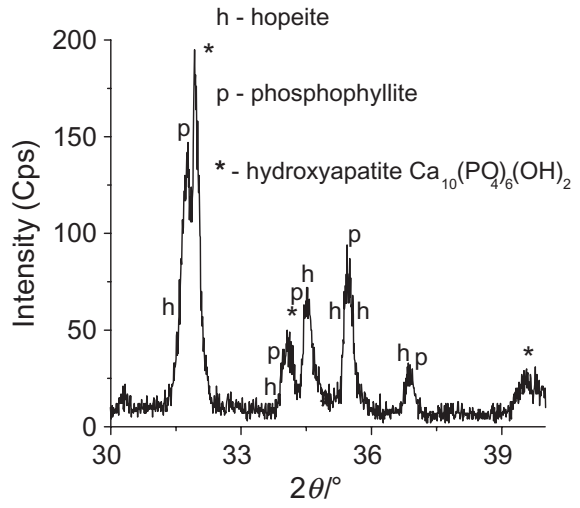

Figure 12. X-ray diffraction pattern of coated steel after 8 days of immersion in S solution.

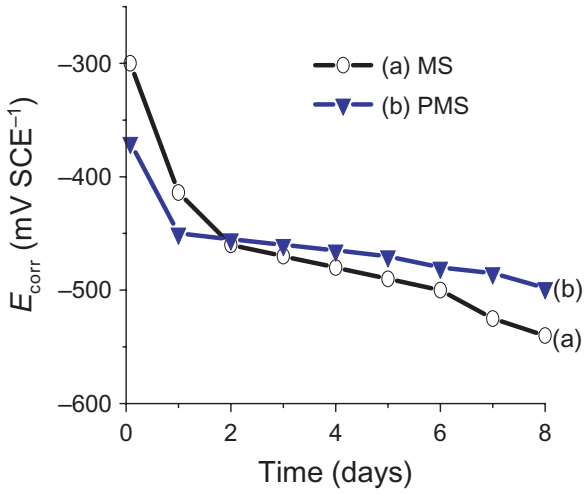

Figure 13. E_{corr} evolution for (a) MS and (b) PMS in SC solution.

SEM observations and surface analyses (EDS and XRD) confirm the electrochemical impedance results and show that the changes at the coated steel surface improve the anticorrosive properties of the coating obtained by chemical conversion.

3.3. Corrosion behaviour in alkaline medium contaminated by chloride (SC)

3.3.1. Corrosion potential evolution. Figure 13 shows the E_{corr} evolution of the PMS and MS samples during the immersion in an alkaline medium contaminated by chloride. The E_{corr} of MS samples decreases (figure 13(a)) and stabilizes to $-550\,mV\,SCE^{-1}$ after 8 days of immersion. This evolution corresponds to an active state of the steel. For the coated steel, the decrease in E_{corr} is slower and after 2 days of immersion, the E_{corr} values are slightly higher than those of MS.

The comparison of these results with E_{corr} evolution measured in the S solution (figure 4) shows that the PMS sample is subject firstly to coating deterioration by medium alkalinity, and secondly to steel corrosion through open pores of the coating.

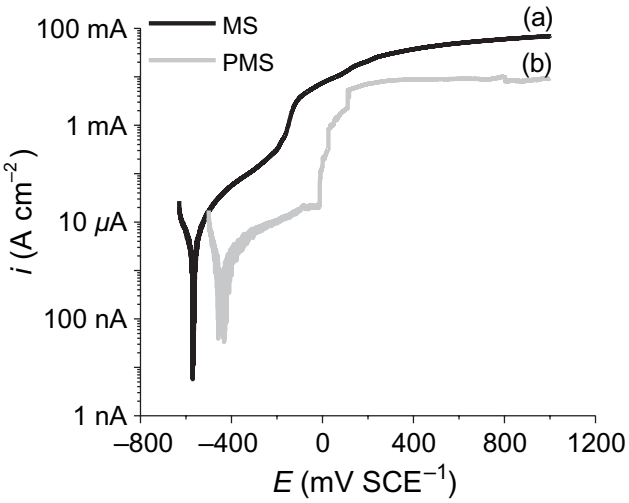

Figure 14. Polarization curves for MS and PMS after 8 days of immersion in SC solution.

Table 7. Corrosion potentials, current densities (at corrosion potential) and pitting potentials of MS and PMS samples after 8 days of immersion in SC solution.

Sample	E_{corr} (mV ECS^{-1})	i (μA cm^{-2})	E_{pit} (mV ECS^{-1})
MS	−570	20	−180
PMS	−460	2	−20

3.3.2. Polarization curves. The polarization curves of both PMS and MS samples after 8 days of immersion in the SC solution are shown in figure 14. A potential shift of 110 mV is observed between the coated and uncoated steels.

Increases in passive current density with the modified pitting potential from 560 to $-80\,mV\,SCE^{-1}$ (for MS) and from 556 to $-20\,mV\,SCE^{-1}$ (for PMS) were observed. The drop of one decade in current density at the corrosion potential of PMS with respect to that of MS shows the positive role of the zinc phosphate coating obtained by CC. The measured current density (at corrosion potential) reaches a reproducible value of 2 $\mu A\,cm^{-2}$ (table 7).

In conclusion, after 8 days of immersion in the SC solution, PMS shows a lower current density than MS, and decreases the pitting susceptibility by increasing pitting potential at about 160 mV compared with MS.

3.3.3. EIS. The electrochemical impedance diagrams (Nyquist and Bode) of the steel and coated steel obtained at the corrosion potential after 1 and 8 days of immersion in the SC solution are shown in figure 15. These diagrams present one capacitive loop for steel and two non-decoupled capacitive loops for the coated steel. The equivalent electrical circuit indicating the all phenomena detected during the 8-day immersion has one time constant for the steel (figure 7) and two time constants for the coated steel (figure 9(a)). The

Table 8. Electrical parameters of MS and PMS immersed in SC solution obtained by fitting EIS data.

Sample	Time (day)	R_F (kΩ cm^2)	α_F	C_F (μF cm^{-2})	R_t (kΩ cm^2)	α_{dl}	C_{dl} (μF cm^{-2})	χ^2 (error factor)
MS	1	–	–	–	7.9	0.92	60.6	4.4×10^{-3}
	4	–	–	–	3.8	0.88	60	9×10^{-3}
	8	–	–	–	3.4	0.89	62.5	6.6×10^{-3}
PMS	1	36.2	0.7	1.3	50.7	0.9	36.3	4×10^{-3}
	4	4	0.8	6.9	27.5	0.9	41.7	4×10^{-3}
	8	4.8	0.8	6.4	20.7	0.9	58	4.4×10^{-3}

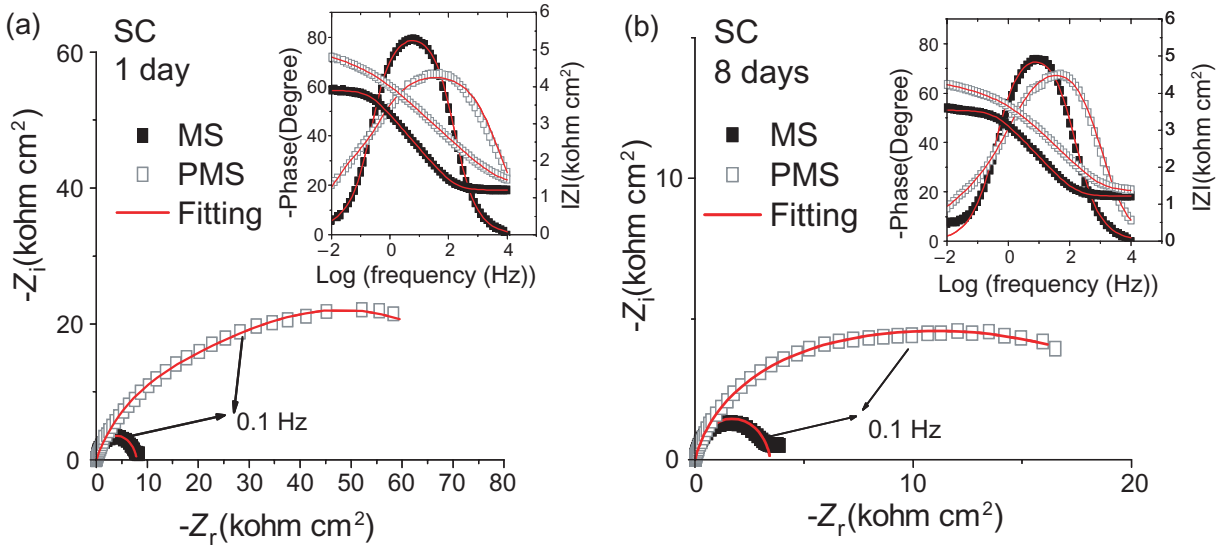

Figure 15. Nyquit and Bode diagrams of MS and PMS, experimental values (dots) and fitted values (solid line), after (a) 1 and (b) 8 days of immersion in SC solution.

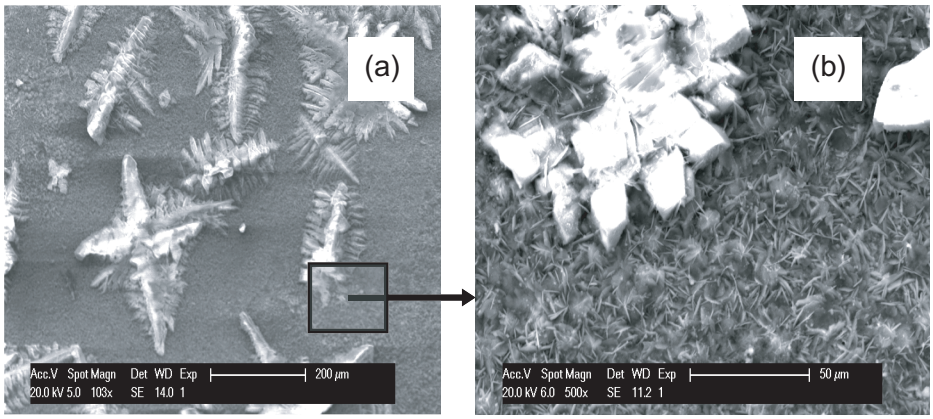

Figure 16. SEM images of PMS after 8 immersion days in SC solution: (a) 200 and (b) 50 μm scales.

electrical parameters obtained after modelling EIS data are listed in table 8.

The impedance diagram evolution (figure 15) with immersion time shows that the chloride presence in the SC solution simultaneously results in a competition between the formation and local destruction of the film obtained by the slow coating dissolution. This classical corrosion mechanism leads to an R_t decrease and an increase in the double layer capacitance C_{dl} Note that during immersion, for PMS samples, R_t remains higher than that for MS samples. R_F is the electrical resistance of ion transfer through open coating pores. It decreases with time: this evolution corresponds to electrolyte diffusion into the coating pores.

In the case of PMS, the film morphology is similar to that observed in the absence of chloride ions (figure 10) and the x-ray diffraction pattern shows the presence of hydroxyapatite $Ca_{10}(PO_4)_6(OH)_2$ Thus, hydroxyapatite formation occurs even in the presence of chloride ions (figure 16). Compared with that of MS, the formation of this film due to the slow dissolution of the coating deposited before, leads to a better protection of the steel, as shown by EIS diagrams (figure 15).

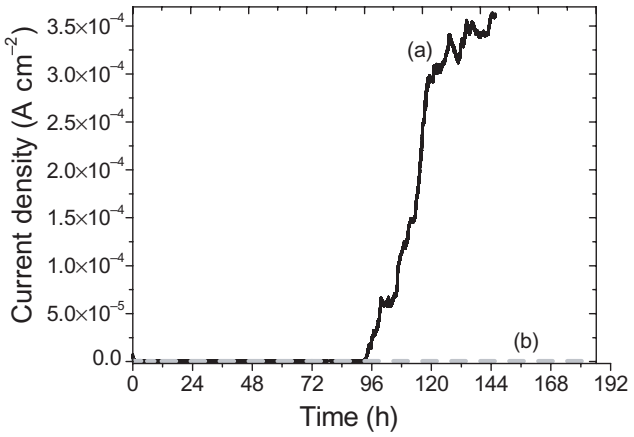

Figure 17. Current density evolution of (a) MS and (b) PMS embedded in mortar.

3.4. Corrosion behaviour in concrete

Figure 17 shows the evolution of the current density of the two reinforced mortar specimens (PMS and MS). At the beginning of the tests, the pH in the vicinity of the rebars embedded in mortar exceeds 12. For the mild steel embedded in mortar, the evolution of corrosion current density i_{corr} (figure 17(a)) shows that at the beginning of immersion, almost constant values less than $1\,\mu A\,cm^{-2}$ are obtained. After 95 h of immersion, an increase in i_{corr} occurs up to $0.4\,mA\,cm^{-2}$. These values show that at the beginning of the tests, the steel is in a passive state, whereas after ∼4 days of immersion, it is in an active corrosion state ($i_{corr} > 1\,\mu A\,cm^{-2}$).

The increase in current density shows that the concentration of chloride at the steel/concrete interface exceeds the critical threshold $[Cl^-]/[OH^-] = 0.6$ which leads to the start of corrosion and the accumulation of corrosion products [19, 20]. These corrosion products generate micro- and macro-cracks in concrete [1]. Thus, after 120 h of immersion, these cracks and disseminated corrosion products become visible to the naked eye (figure 18). The coated sample has $i_{corr} < 0.5\,\mu A\,cm^{-2}$ throughout the test. These results show that the phosphated surface plays an important role in protecting against steel and concrete damage. The coating aspect after this test (figure 19(b)) shows no rust or localized attack on the coated steel. The SEM images of the PMS sample show the formation of small hexagonal crystals

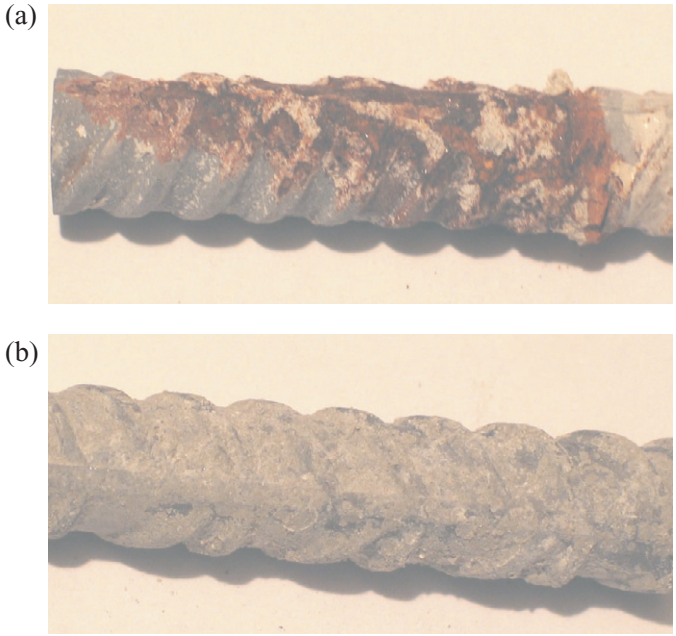

Figure 19. (a) MS and (b) PMS observations after removal of the mortar.

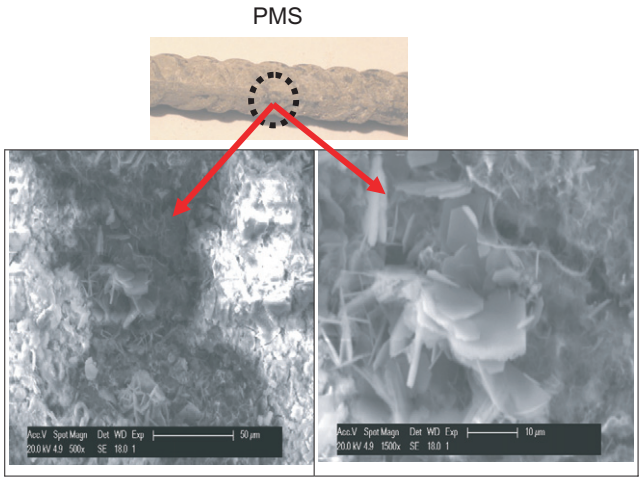

Figure 20. SEM images of mild steel coated surface after removal of mortar.

at the phosphate coating/concrete interface (figure 20). These crystals are identical to those observed in a simulated concrete solution contaminated by chlorides. Results of the

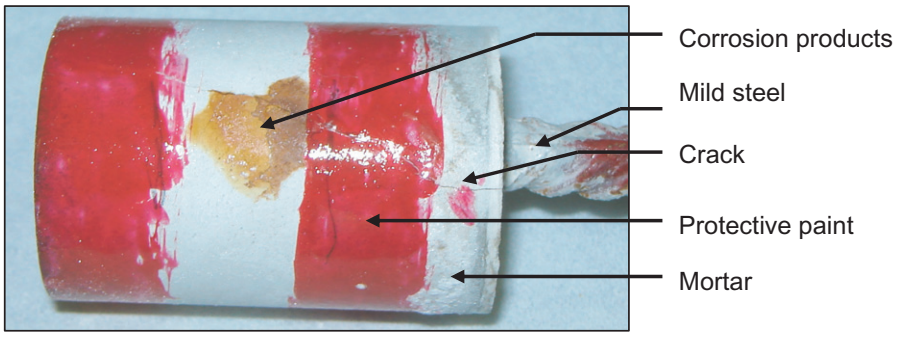

Figure 18. MS embedded in mortar after 144 h of immersion in 3.5% NaCl solution and at an imposed potential of 400 mV SCE^{-1}.

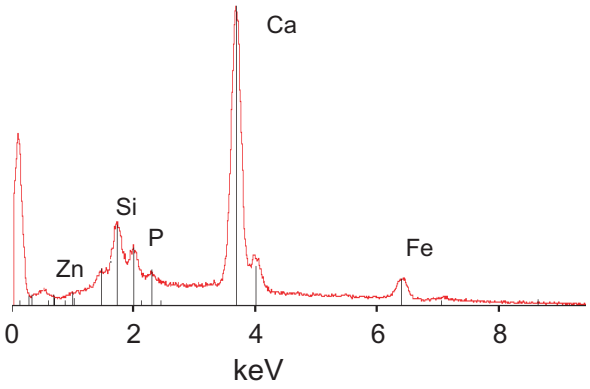

Figure 21. EDS composition of PMS after removal of mortar.

EDS show that these crystals are composed of P, O and Ca (figure 21).

Indeed, EDS confirms that the zinc phosphate coating protects the reinforcement and delays the initiation of its corrosion when the interstitial concrete pore solution is contaminated by chlorides. Thus, the tests here revealed the potential of phosphate treatment in concrete rebar protection.

4. Conclusion

New protective coatings have been developed by chemical conversion (CC) in reinforcing bars to prevent its corrosion in concrete. The coatings obtained using the phosphate process are composed of two phases: hopeite and phosphophyllite.

In alkaline solutions with or without chloride, a phosphated mild steel sample (PMS) is more resistant than mild steel (MS) alone. Indeed, this study showed that, during the first immersion days in alkaline media (pH = 22.6), a slow dissolution of the coating occurs. Zinc phosphate coating dissolution is accompanied by hydroxyapatite $Ca_{10}(PO_4)_6(OH)_2$ formation. Hydroxyapatite appears with formation of a phosphate layer, a dense and protective coating.

In a chloride ion solution, at very high concentration exceeding the chloride threshold accepted for steel corrosion in alkaline media ($[Cl^-]/[OH^-] > 0.6$). The hydroxyapatite film resulting from phosphate coating dissolution contributes to the reduction in chloride aggressiveness and provides an effective protection against the corrosion of steel reinforcement.

References

[1] Assouli B, Simescu F, Debicki G and Idrissi H 2005 *NDTE Int.* **38** 682
[2] Manna M, Chakrabarti I and Bandyopadhyay N 2006 *Surf. Coat. Technol.* **201** 1583
[3] Manna M, Bandyopadhyay N and Bhattacharjee D 2008 *Surf. Coat. Technol.* **202** 3227
[4] Bikulčius G, Girčiene O and Burokas V 2003 *Russ. J. Appl. Chem.* **76** 1759
[5] Weng D, Jokiel P and Uebleis AB 1996 *Surf. Coat. Technol.* **88** 147
[6] Donofrio J 2000 *Met. Finish.* **98** 57
[7] Ogle K, Meddahi N, Tomandl A and Wolpers M 2003 *Proc. 1st Int. Surface Treatments Institute of Franche-Comté Conf. Automotive Industry, France*
[8] Ogle K, Tomandl A, Meddahi N and Wolpers M 2004 *Corros. Sci.* **46** 979
[9] Tomandl A, Wolpers M and Ogle K 2004 *Corros. Sci.* **46** 997
[10] Li G Y, Niu L Y, Lian J S and Jiang Z H 2004 *Surf. Coat. Technol.* **176** 215
[11] Shoeib M, Farouk M and Hanna F 1997 *Met. Finish.* **95** 62
[12] Kouisni L, Azzi M, Zertoubi M, Dalard F and Maximovitch S 2004 *Surf. Coat. Technol.* **185** 58
[13] Jegannathan S, Sankara Narayanan T S N, Ravichandran K and Rajeswari S 2006 *Surf. Coat. Technol.* **200** 4117
[14] Sinha P K and Feser R 2002 *Surf. Coat. Technol.* **161** 158
[15] Andrade C, Keddam M, Novoa X R, Perez M C, Rangel C M and Takenouti H 2001 *Electrochim. Acta* **46** 3905
[16] Meroufel A, Deslouis C and Touzain S 2008 *Electrochim. Acta* **53** 2331
[17] Rout T K, Bandyopadhyay N and Venugopalan T 2006 *Surf. Coat. Technol.* **201** 1022
[18] Shih W, Chen Y, Wang S, Li W, Hon M and Wang M 2005 *J. Cryst. Growth* **285** 633 J
[19] Idrissi H and Limam A 2003 *NDT&E Int.* **36** 563
[20] Huet B, L'Hostis V, Santarini G, Feron D and Idrissi H 2007 *Electrochim. Acta* **49** 1918